Effect of Combined ASR and Cyclic Loading on Concrete Bridges

Salhin M. Alaud[1(✉)] and Gideon P.A.G. van Zijl[2]

[1] Civil Engineering, El-mergib University, Al Khums, Libya
salhin.alaud@gmail.com
[2] Civil Engineering, Stellenbosch University, Stellenbosch, South Africa
gvanzijl@sun.ac.za

Abstract. Reinforced concrete beams were subjected to the combination of mechanical loading and alkali-silica reaction (ASR) in order to investigate the durability of concrete under their combined action. This experiment used locally-sourced materials such as aggregates and admixtures in order to develop a concrete mix that will give the optimum resistance to such combined action. Half of the specimens were subjected to static, and cyclic loading and exposure to accelerated ASR-inducing environment and the other half were exposed only to an ASR-inducing environment. The test results indicate that the expansion due to the combined action was significantly different from that in specimens exposed only to a high-alkaline environment. The micro and macro cracks induced by cyclic loading form paths leading to an increased ASR rate, while the macro-mechanical cracks provide regions of relatively free expansion, as can be deduced from the decreasing crack widths.

Keywords: Reinforced concrete · Alkali-silica reaction · Cyclic loading · Crack width · Combined action

1 Introduction

It is known that ASR occurs in concrete due to the presence of reactive silica in aggregates which react with alkali in cement or from other resources, creating a low-volume gel which induces volume increase, cracking and deterioration of concrete. The gel produced by ASR expands into pores and cracks in the cementitious skeleton, being in a sufficiently humid environment (Bangert and Meschke 2001). At a later age, some substances from the leaching of calcium hydroxide into concrete could block small pores on the surface of the concrete, thereby decreasing the permeability (Wang et al. 1997). Mechanical loads may also cause cracks in concrete, for instance in the form of cyclic loads on bridge girders by heavy vehicles. Cracks allow more water (Wang et al. 1997) or aggressive chemical ions to penetrate into the concrete, facilitating deterioration. Most researchers consider that a concrete containing discontinuous pores and microcracks is well designed and manufactured. An important role in the macroscopic expansion of concrete structures is played by microcracks. The macroscopic expansion almost may be not observed when the gels find enough space to expand without cracking the cement paste (Charpin and Ehrlacher 2012). Mechanical

H. Rodrigues et al. (eds.), *Facing the Challenges in Structural Engineering*,
Sustainable Civil Infrastructures, DOI 10.1007/978-3-319-61914-9_16

cracking when the concrete structure is also loaded plays an important role concerning the anisotropy of ASR expansion. Many researchers suggested that pozzolanic materials are important to reduce this expansion. The mature alkali silicate generated from the admixtures fills the micro-pores and thus acts both as ASR inhibitors and pozzolanic material (Ichikawa 2009).

In many cases, several deleterious mechanisms will act simultaneously or consecutively, thus contributing to the damage of the concrete. The presence of pavements in the proximity of high humidity such as river bridges, where exposure to dynamic loadings often cause cracks and contribute to the ingress of water and humidity in concrete. These structures will be exposed to combined mechanical loading and ASR action. To simulate the structures in or close to water and/or high humidity, reinforced concrete elements containing a high alkaline level were cast and submerged partially in water according to (ASTM C1293 2008). In order to investigate the effect of mechanical cracks on ASR progress, cyclic loading on the specimens was applied. The purpose was to determine the influence of the mechanical load on ASR in reinforced concrete.

2 Combined Cyclic Load and ASR

Structures are influenced by internal and external processes. The internal actions are dependent on the physical properties of concrete materials and the chemical reactions between the components during the hydration process, or later due to a slow reaction caused by external factors. The external factors are mechanical loading and environmental actions such as humidity, temperature, chloride and carbon dioxide. No accepted technical method for verifying the structural response to environmental exposure while under mechanical loading is available at present. The reinforced concrete structures nearby or in water (sea, river,…etc.) are more vulnerable to the combined actions. Cyclic loading (waving vehicles and ships in motion) and ASR in the presence water or high humidity could simulate these conditions. Only a few researchers have studied the combination of cyclic loading and environmental action. A research programme of reinforced concrete elements subjected to cyclic loading and corrosion was conducted by (Giordano et al. 2011). They monitored the growth of cracks due to this combined action and observed that the accumulation of the damage is significantly different when cycling action is combined with a chemical attack. The fatigue behaviour for plain concrete including ASR in flexure, compression as well as under repeated indirect tensile stress has been studied by (Ahmed et al. 1999). They found that the ASR cracks significantly affect the modulus of rupture of concrete specimens and therefore reduce the fatigue life of the concrete. In the previous investigations, no fundamental explanation was found for the response of reinforced concrete to ASR under cyclic mechanical loading, which will be considered in this paper. The idea is to partially submerge reinforced concrete prisms that contain high alkali content and reactive aggregate, and which have been exposed to cyclic tensile leading to cracking, in water. The other sides of the prisms which are not in water are exposed to high humidity.

3 Experimental Program

The experimental programme was performed to investigate the expansion and behaviour of reinforced concrete containing Greywacke and Granite aggregates under combined action.

3.1 Materials

Reactive and non-reactive aggregates namely Greywacke and Granite stone (Giordano et al. 2011; Ichikawa 2009) from different locations in the Western Cape region of South Africa were used throughout the research. Philippi local fine dune sand was used as fine aggregate. A Pretoria Portland cement (PPC) type CEM I 52.5 N was used, and ground granulated corex slag (GGCS) replaced 50% of the cement (by mass) in half of the samples. The equivalent sodium oxide Na_2Oe (Na_2O + 0.658 K_2O) in the cement used was 0.60%. Sodium hydroxide was dissolved in the mixing water in order to increase the Na_2Oe content to 1.25% of the mass of cement. The coarse aggregate gradation for Granite and Greywacke stone was 1/3 each of size 13 to 19 mm, 9.5 to 13 mm and 4.75 to 9.5 mm. The specimens (prisms) were centrally reinforced with a single ribbed steel bar of 16 mm Ø. The yield (fy) and ultimate strength (ft) of the steel were 480 MPa and 531 MPa respectfully.

3.2 Test Specimens and Devices

Prisms of concrete with a length of 350 mm, a square section with sides of 100 mm were made. In order to anchor and perform the tensile and cyclic mechanical loading, the reinforced steel was threaded at both ends that protruded from the specimen. In order to ensure crack formation in the middle of the specimen, the 50 mm long central part of the 16 mm diameter steel bar was reduced to a diameter of 13 mm. The dimensions and shape of the beam and reinforced steel is illustrated in Fig. 1. Four mixes were cast and indicated by Gw, Gn, Gw-co and Gn-co (Gw = Greywacke mix, Gn = Granite mix and -co-refers to corex slag in a mix). The mix proportions by weight are shown in Table 1. A total of 36 specimens were cast from the two

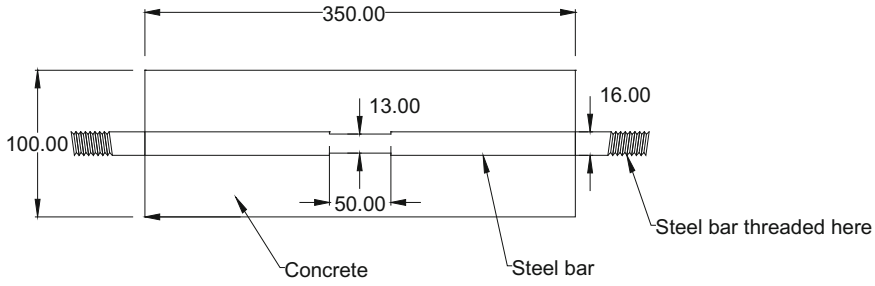

Fig. 1. Details and dimensions of test specimen

Table 1. Concrete mix proportions (kg)

Mix	Cement CEM I 52.5	Corex slag	Granite stone	Greywacke stone	Philippi sand	NaOH	Water
Gw	440	–	–	1000	815	5.63	208
Gn	440	–	1000	–	–	5.63	212
Gw-co	220	220	–	1000	815	5.63	212
Gn-co	220	220	1000	–	–	5.63	216

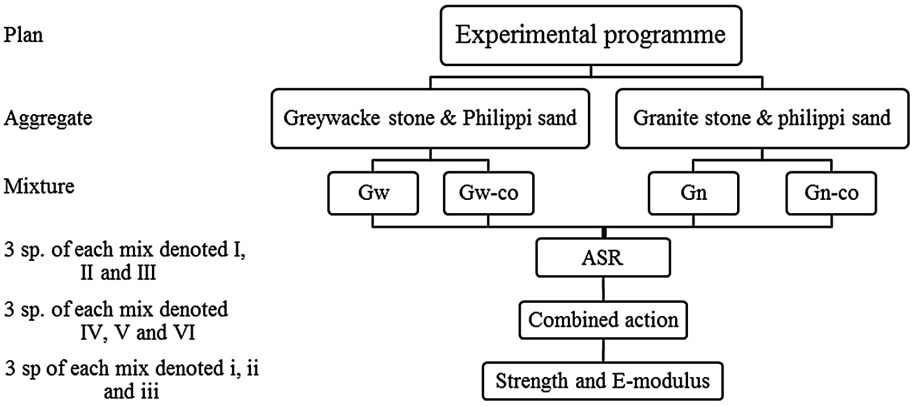

Fig. 2. Flow-chart of experimental plan

aggregates, with 18 specimens being cast from Greywacke stone, nine of them containing 50% of corex slag and the other 18 specimens from Granite stone, nine of them also containing 50% of corex slag. Six samples of each mix made were divided to 3 specimens under ASR action that were marked with I, II and III, and 3 specimens subjected to combined action that were marked IV, V and VI. The other three specimens of each mix named i, ii and iii were made to determine the yield and ultimate tensile strength. A flowchart in Fig. 2 illustrates the plan of the experimental steps.

A chamber was designed to immerse the specimens partially in the water and expose the upper half to humidity. The Instron MTM was used to perform the cyclic load test, and to record the loading applied. To subsequently accurately measure the crack widths on the surface, high-resolution photos were taken with a DigiMicro Mobile (dnt) camera with 10 × 500 magnification and 12 megapixels. A strain gauge (Marcator 1075R 12.5 mm 0.001) was used to measure the change in strain over time.

3.3 Test Procedure

This experiment was conducted at the laboratory of Civil Engineering Department, Stellenbosch University.

3.3.1 Casting and Set-up

Steel moulds were used for all the specimens cast and externally vibrated using a table vibrator. After troweling the concrete surface smooth, the specimens were covered with plastic sheeting and left under laboratory conditions for 24 h. After de-moulding, the external steel bars were covered by rubber caps made especially for them. To assure that there was no entry of water into the specimen, which would lead to corrosion, grease was applied to the protruding bars under the rubber cover. The samples i, ii and iii were completely submerged in water at 23 ± 2°C until shortly before conducting static, monotonic tensile tests on them at the age of 28 days to determine their yield and ultimate strength. The average of yield and ultimate load was recorded and the results of the four mixes were convergent. The average of the yield and ultimate load of these mixes were 88.3 kN and 91.28 kN respectively. To monitor deformation during the combined tests of ASR and cyclic loading, eight stainless steel datum disks (pins) were glued onto two opposite sides of the samples I, II, III, IV, V and VI (four on each side), spaced 100 mm apart, to monitor the change in the concrete length. The spaces between the pins were numbered 1, 2 and 3 on one side and 4, 5 and 6 on the other side. The specimens were left to enable the glue to dry (6–7 h) before measuring the spaces between the pins (zero reading). After the zero readings were taken, the specimens were placed vertically on a Perspex base in a specially built chamber at a height of 100 mm from the bottom in order to submerge the bottom half in water and keep the top half exposed to high humidity (>90%) at 38°C. The three spaces were under three conditions: the lower spaces (1 & 4) were totally submerged in water, the lower half of the middle spaces (2 & 5) were submerged and the upper were exposed to humidity, and the upper spaces (3 & 6) were exposed to humidity. Figure 3 shows placing of the specimens on the base in the chamber, the numbers of the spaces between the pins, samples denotation and the condition. Elements connected to the device were set at a

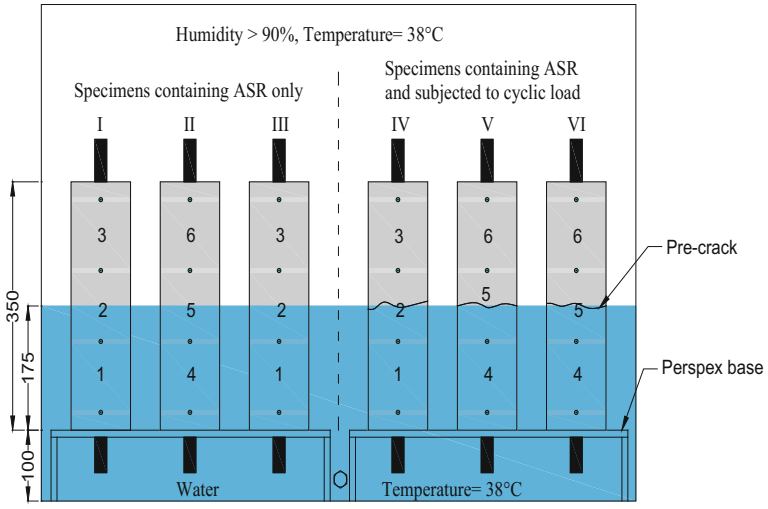

Fig. 3. Placement of the specimens on the device (6 of each, 4 mixes)

temperature at 38°C according to ASTM C 1293. To keep the level of water constant, a float was connected to compensate for the loss of water. From each of the four mixes, the specimens denoted I, II, and III were left in the described accelerated ASR exposure condition (ASR) and the ones named IV, V, and VI were subjected to cyclic loading with ASR (combined action) at 28 days.

3.3.2 Cyclic Loading and Measuring

A tensile load was applied to the specimen's number IV, V and VI of up to 62 kN which represent 70% of the yield load (specimens i, ii and iii) to obtain cracks in the middle and then 100 000 cycles were applied with a 5 Hz frequency. These mechanical tests were conducted on Gw and Gn specimens after 4 weeks and on Gw-co and Gn-co after 15 weeks after being extracted from the device and after the deformation between the spaces were recorded. Figure 4a shows the relationship between displacement and load, and Fig. 4b shows the average displacement at the upper range of the load cycle, versus the number of cycles. After the load cycles, the deformation readings were taken again and recorded, after which specimens were returned to the device in the same condition. The deformation of all specimens and crack widths of the combined specimens were measured subsequently at regular intervals, at a specific time after removing the specimens from the device and returning them to the chamber after 40 to 60 min. The dnt camera was used to measure the crack widths, using a specially supplied program, considering the magnification factor that was used when the photo was taken. The photos were carefully taken in the exact same positions. Deformation and crack width results were recorded in this way over a total period of 15 months and subsequently represented in graphs.

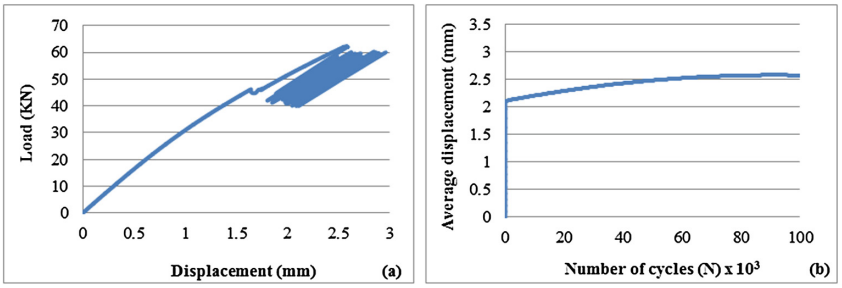

Fig. 4. An example of the cyclic load for Gw/w specimens: (a) the cyclic load and displacement, (b) the average displacement and number of cycles.

4 RESULTS

The mechanical load causes macro cracks in the middle of the specimens as planned. These cracks had different widths on the surface of the various specimens (about 0.6 to 1.8 mm) and extended through the cross section down to the steel bar. Microcracks could also have been caused in the skeleton of concrete due to cyclic loading. The average crack widths and expansions in the specimens are summarized in Table 2.

Table 2. Expansions and initial mechanical crack widths in the specimens (mm)

Mix specimens	Initial crack width (mm)	Average expansion in specimens (%)			
		Calculated from start of test		Calculated after mechanical crack	
		Combined	ASR	Combined	ASR
Gw	1.83 (0.02)	0.725	0.195	0.129	0.184
Gn	1.82 (0.3)	0.67	0.097	0.031	0.087
Gw-co	0.89 (0.07)	0.38	0.010	0.038	0.054
Gn-co	0.64 (0.17)	0.197	0.057	0.023	0.022

4.1 Greywacke Mixes (Gw)

ASR cracks developed in specimens for the Gw mix (both of ASR and combined), and could be seen clearly in the submerged part, but were smaller in the upper part which was exposed to high humidity and capillary water. In specimens IV, V and VI, the mechanical crack in the middle increased the deformation dramatically over measurement regions 2 and 5 after the load was applied, and then started decreasing with time. The average strain readings (average of measurements over cracked and un-cracked spaces 1, 2, 3, 4, 5, 6) in ASR specimens I, II and III, and in combined specimens IV, V, VI are shown in Fig. 5. The strain increased steadily under the ASR condition, whereas under the combined action it increased before the mechanical load was applied, and then became less significant than in the ASR condition. The maximum expansion for Gw from the first day until 65 weeks was about 0.195% in the ASR specimens, and about 0.725% in the combined specimens as in Fig. 5a. It can be noted that the expansion under combined action is significantly larger than in ASR specimens, because of including the mechanical crack in the former specimens. If the strain change is considered after the mechanical load that was applied at four weeks, i.e. if changes in deformation after this time only are converted to strain and presented on a graph (Fig. 5b), the maximum strain of ASR specimens was 0.184% and 0.129% in the combined specimens.

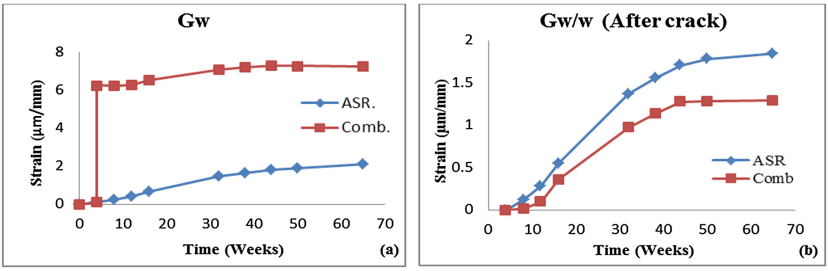

Fig. 5. Strain against time for the Gw specimens subjected to ASR (I, II, III) and exposed to combined action (IV, V, VI): (a) from the start of the test and (b) after cyclic loading at 4 weeks.

4.2 Granite Mixes (Gn)

The strain in Gn mixes was less than that in Gw mixes, where the Granite mixes classify as non-reactive or slowly reactive. The average strain readings of six spaces of each of three specimens in both cases of Gn mixes were recorded. A lesser expansion was recorded in upper part which was exposed to humidity than in the lower part which was submerged. The strain jumped after cyclic loading in the combined specimens, and then became less than the strain in ASR specimens. In Fig. 6a, the maximum strain at 65 weeks in ASR specimens was around 0.097%, while the strain due to mechanical cracking and ASR in combined specimens was 0.67%. The strain development after cyclic loading as illustrated in Fig. 6b was greater in ASR than in combined specimens due to mechanical crack spaces which allowed expansion into the crack dimension. In this case, the maximum strains were 0.0873% and 0.0308% in ASR and combined specimens respectively. The strain increased steadily in both cases and then became less after 16 weeks. The strain percentages between the combined and ASR conditions gradually diverge in the first stages and then become semi- stationary over time.

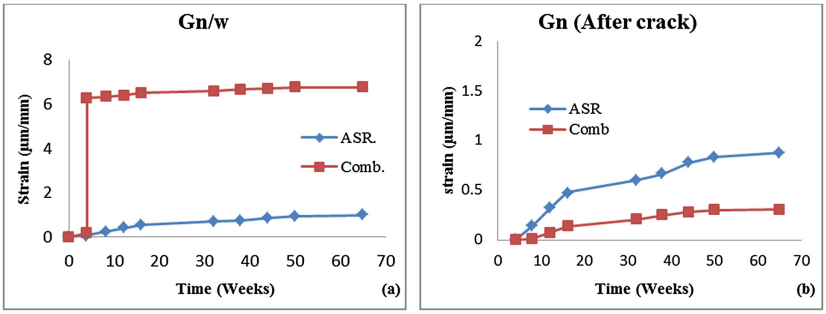

Fig. 6. Strain against time for the Gn specimens subjected to ASR (I, II, III) and exposed to combined action (IV, V, VI): (a) from the start of the test and (b) after cyclic loading at 4 weeks.

4.3 Greywacke with Corex Slag Mixes (Gw-Co)

The cyclic loading was applied on the combined specimens after 15 weeks of being partially submerged in water caused crack in the middle of specimens increased the total strain in the combined action condition. Figure 7a illustrates the strains in both ASR and combined mixes of Gw-co from the start of the test until 65 weeks. The maximum strains were about 0.1% in ASR and 0.38% in combined specimens including the large mechanical crack. Figure 7b represents the strain in both cases after cyclic loading and, as in Figs. 5b and 6b, regards this point of strain to be equal to zero. In this case, the maximum strains at the 65th week were 0.054% and 0.0377% in ASR and combined mixes respectively.

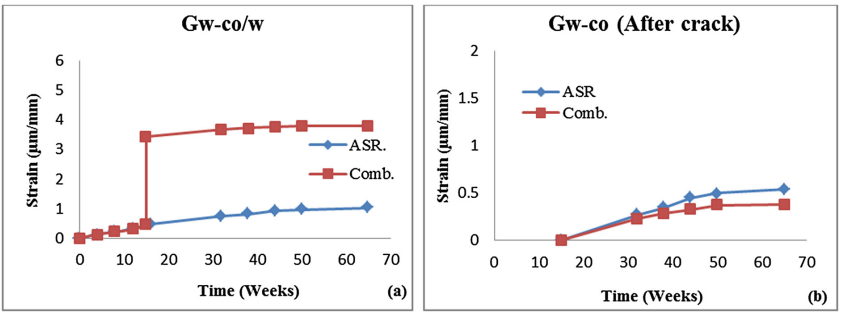

Fig. 7. Strain against time for the Gw-co specimens subjected to ASR (I, II, III) and exposed to combined action (IV, V, VI): (a) from the start of the test and (b) after cyclic loading at 15 weeks.

4.4 Granite with Corex Slag Mixes (Gn-Co)

As in previous mixes, the mechanical load was applied on the specimens IV, V and VI of Granite mix with corex slag (Gn-co) after 15 weeks of casting. The difference in strain between Gn and Gn-co can be noted in the results, where the strain in the presence of corex slag was less than that in Gn. The average strain readings of the spaces and of the three specimens in both cases of Gn-co mixes were recorded. The strain after the cyclic loading in combined specimens was less than that in Gn due to the crack width. The maximum strain in ASR and combined specimens from the start of the test until the 65th week were 0.057, and 0.2% respectively as shown in Fig. 8a. The strain measured after cyclic loading was applied in the combined specimens (i.e.16 weeks) were recorded at the 65th week as 0.022% and 0.023% for ASR and combined specimens respectively. As in Fig. 8b, the strain in the combined specimens was slightly smaller than that in the case of ASR throughout the weeks.

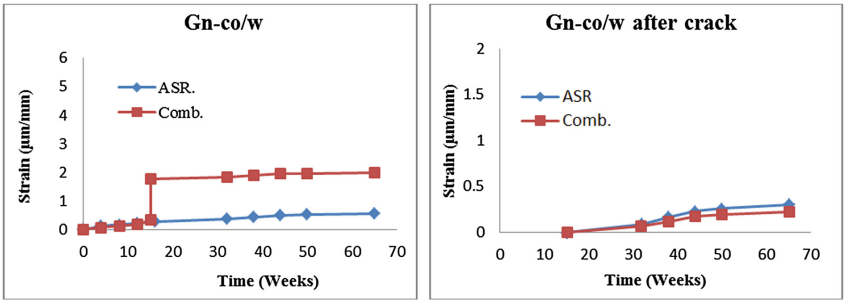

Fig. 8. Strain against time for the Gn-co specimens subjected to ASR (I, II, III) and exposed to combined action (IV, V, VI): (a) from the start of the test and (b) after cyclic loading at 15 weeks.

4.5 Mechanical Crack Width

The mechanical crack width plays a significant role in subsequent concrete volume changes. In the case of ASR expansion, the crack will provide space for concrete to expand. To determine the change in the pre-cracked concrete, the previously mentioned dnt camera was used. At the first reading, the position of measuring was marked to serve as a reference for subsequent reading. The first reading in Gw and Gn specimens was at the 10th week, while in the Gw-co and Gn-co specimens it was at the 16th week. Figure 9 illustrates the reduction of mechanical crack widths in the middle of specimens. The reduction due to certain factors (ASR expansion, self-weight of upper part of the specimen and temperature) was different in the four mixes. The largest reduction was in Gw, where the maximum reduction at the 65th week was around 23.7% of the crack width at the 10th week. In Gw-co, the reduction was less than in the Gw mixes, where the maximum reduction was 8.7%. In Granite mixes, the reductions at the end of the test were 7.9% and 8.7% in Gn and Gn-co respectively. Figure 10 illustrates the stages of the reduction in the mechanical cracks of Gw and Gn mixes over time, and the stages of Gw-co and Gn-co are illustrated in Fig. 11. In Fig. 10 the increase in ASR cracks, i.e. the fine, vertical cracks in the Gw mix can be seen.

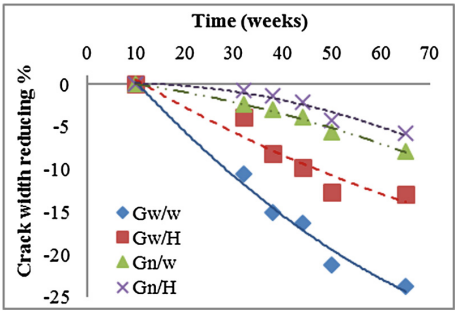

Fig. 9. Mechanical crack widths reducing over time

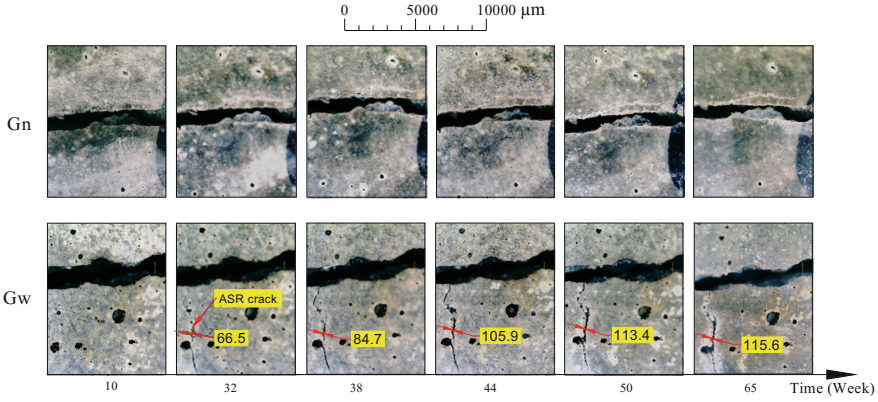

Fig. 10. Mechanical and ASR cracks changing over time in Gw and Gn mixes

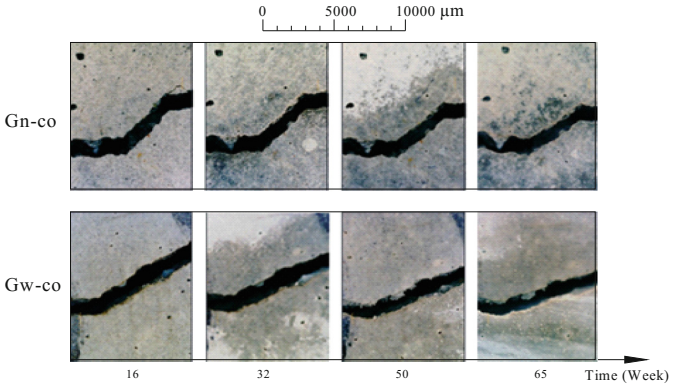

Fig. 11. Mechanical cracks changing with the time in Gw-co and Gn-co mixes

4.6 ASR Crack

The formed gel starts expanding into pores and microcracks of the cement matrix. As it fills up the available space, it exerts a pressure on the surrounding skeleton. ASR cracks appeared in Greywacke mixes (Gw) of ASR and combined specimens (I to VI) at the 32^{th} week. The main cracks often form in the reinforced steel direction and the crack branches in a perpendicular direction. ASR micro cracks were only seen at 44 weeks in Gn mixes, while there were no cracks observed after 65 weeks in the mixes with GGCS (Gw-co and Gn-co). The vertical crack in lower photos in Fig. 10 shows the ASR cracks increasing with the time in Gw specimens.

5 Discussion

The pre-cyclic loading of concrete prisms has been shown to exert a significant influence on crack widths and the strain of ASR-affected concrete. The formation of an ASR gels usually occurs in the case of pre-existing degradations and ASR cracks mainly result from constructive weaknesses, as well as the ability of the silica in the aggregate to interact with alkali.

Throughout the results shown in Figs. 5, 6, 7 and 8 the strains in combined specimens were less compared to the samples that were not mechanically cracked. The ASR expansion of both sides (bottom and top) takes place in all directions including in the direction of the crack in the middle. This phenomenon can be caused by the fact that (i) part of the expansion is absorbed by the mechanical cracks in the cracked middle space and that expansion occurs in the sides due to micro cracks being caused by cyclic loading and (ii) that mechanical microcracks interconnect flow paths and increase concrete permeability allowing more water or aggressive chemical ions to penetrate into the concrete, facilitating deterioration (Wang et al. 1997). The large mechanical cracks (i) seem to be the main reason for the decrease in the expansion of the concrete due to the space it offers for concrete to expand. Therefore, the mechanical crack might be useful in this case, but at the same time may lead to impairment of the concrete by other deterioration processes by ingress of deleterious substances.

The stages of strain under combined action are postulated to be associated with the following processes:

1. In the starting reaction, the gel produced fills the small pores before it starts to press on the cement paste.
2. Tensile loading on the beam has an elasticity limit, which may cause cracks in the concrete and, when the load is released, the steel will return, and a concrete crack that is bigger on the external side may remain.
3. Cyclic loading could cause micro-cracks in the concrete beside the main crack, leading to undesirable gases and humidity entering, thereby resulting in more deterioration.
4. After filling the small pores, ASR expansion will be faster until a certain stage and then expand slowly.
5. ASR expansion, thermal expansion, shrinkage and self-weight could contribute to reducing the mechanical crack width and to the expansion of the skeleton of the concrete.

For the experiment, it can be considered that the strains are related to four phenomena: ASR strain ε_{asr}, thermal expansion ε_T, shrinkage ε_{sh}, and mechanical ε_{me}. The total strain in concrete can be decomposed as follows:

$$\varepsilon = \varepsilon_{asr} + \varepsilon_T + \varepsilon_{me} + \varepsilon_{sh} \tag{1}$$

However, it is not quite as simple. The phenomena in Eq. (1) have different mechanisms and depend on certain parameters. For example, in our case, only the upper part of the self-weight of the concrete had an effect on the crack width, while the effect of the other strains came from both directions (upper and lower). Also, all strains in Eq. (1) are a function of time.

The ASR strains are represented by the extent ξ of non-dimensional reaction in kinetic law Ahmed et al. (1999), [12] which can be written as:

$$\xi = 1 - e^{kt} \tag{2}$$

with $\xi \epsilon \{0,1\}$, where the value of $\xi = 0$ is valid when the ASR has not yet started, and $\xi = 1$ represents the case when ASR expansion is complete; k is the characteristic velocity of the process (in constant environmental conditions, often k = constant), and t is the time of reaction.

This law expresses the portion of strain, in the sense that, the ratio must be multiplied by a factor to determine the strain. By meaning, in case free stress, the total strain ε measurable in such an experiment and neglecting the thermal expansion (Temperature is constant) is thus related through a chemical dilatation coefficient β to the extent ξ of the ASR as follows (Ulm et al. 2000):

$$\varepsilon_{asr} = \beta\xi \tag{3}$$

and

$$\beta = \frac{cE_g}{E} \tag{4}$$

where E_g and E are the modulus of elasticity of the gel and the concrete respectively, and c is the intrinsic dilatation coefficient of the reaction products.

In order to model the ASR in concrete induced with a mechanical crack, the period should be divided into two stages: before the mechanical crack and after that. Neglecting the change in cross-section, the longitudinal change Δl in concrete due to ASR and mechanical actions can be described by:

$$\Delta l(t) = \Delta l_i(t_i) + C_w\left(t_{cr}^m\right) + \Delta l_f\left(t_f\right) \tag{5}$$

where Δl_i is the ASR expansion before the mechanical crack, C_w, mechanical crack width, Δl_f, expansion after mechanical crack occurred and t_i, $t_{me,}$ and t_f, the initial reaction time before mechanical crack, mechanical crack time and the final reaction time respectively.

After the mechanical crack arises, the ASR expansion still continues due to retained ASR affinity. The release of restraint to ASR expansion at the crack is believed to induce the subsequent ASR-induced deformed shape shown in Fig. 12. This implies that the overall length in the central gauge area (100 mm of the middle space) will vary as follows before and after the crack is induced:

$$\Delta l = \begin{cases} \beta\left(1 - e^{-kt}\right) l_g & for\, 0 < t > {}_{cr}^{m} \\ \beta\left(1 - e^{-kt_{cr}^m}\right) lg + C_w - 2\beta\left(1 - e^{-k\left(t - t_{cr}^m\right)}\right) l_a & for\, t > t_{cr}^m \, and\, \Delta C_w \le C_w \end{cases} \tag{6}$$

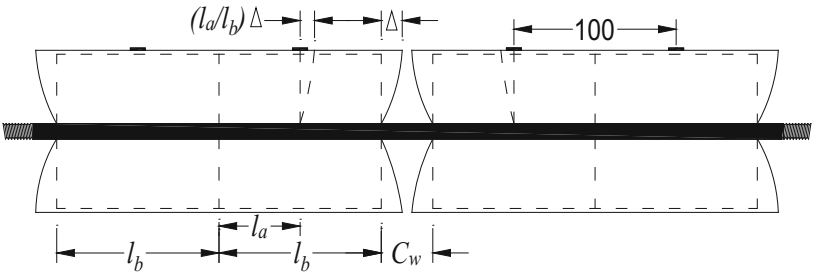

Fig. 12. The deformation mechanism due to combined action

Later, the deformation may close the crack, which means that continued ASR swelling will cause overall lengthening of the gauge length over the crack again from that point onward. This is reflected in the condition of the second part of Eq. (6). The crack will be closed when the deformation in overall crack width $\Delta C_w = 2\beta\left(1 - e^{-k\left(t - t_{cr}^m\right)}\right) l_a = C_w$.

From the same graph, the surface crack width reduction in time can be expressed as:

$$C_w(t) = C_w - 2\beta\left(1 - e^{-k(t-t_{cr}^m)}\right)l_b \quad for\, t > t_{cr}^m \, and \, C_w(t) \geq 0 \tag{7}$$

In Eq. (6), deformation due to self-weight has been considered negligible. Figure 13 illustrates the experimental and computed deformation over the central gauge length due to ASR, and Fig. 14 shows the deformation due to combined action. For different mixes and conditions, k and β values used are given in the figures.

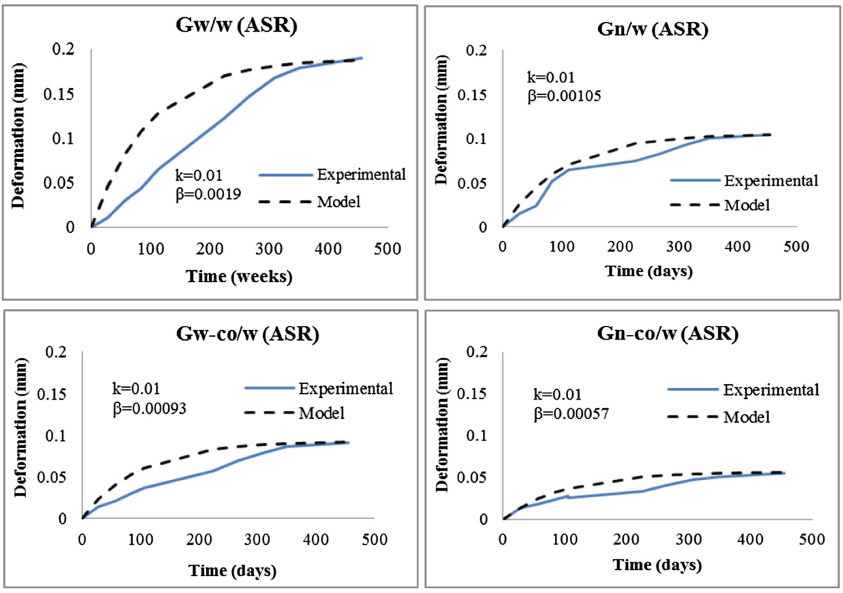

Fig. 13. Experimental and model deformation due to ASR

Note that partial delamination from the steel bar in the cracked region may slightly alter the expression in Eq. (7), as well as the crack shape, also reducing the crack width to an extent at the steel bar interface.

The averages of crack widths C_w were computed from the difference between the total gauge length change before and after the cyclic loading causing the crack. Figure 15 shows the reduction of crack widths computed by Eq. (7) compared with those measured, noting that the widths were measured from the 10^{th} week only in Gw and Gn specimens, while in Gw-co and Gn-co samples they were measured from week 16.

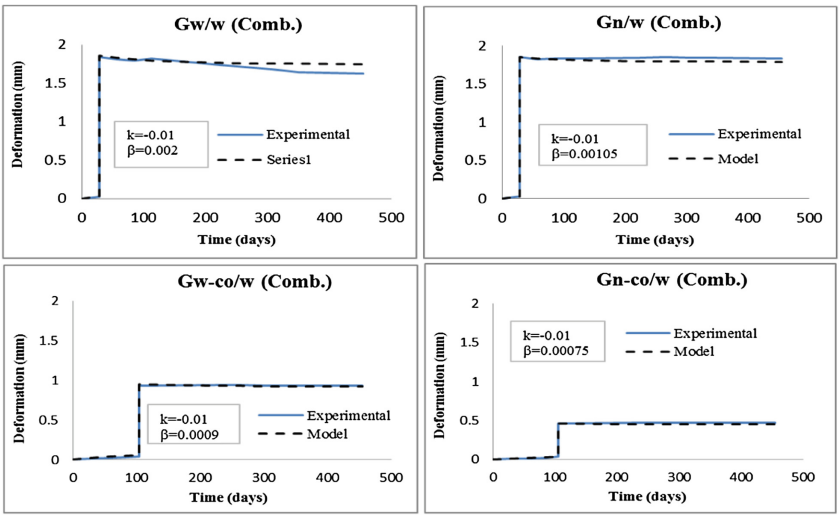

Fig. 14. Experimental and model deformation due to ASR and mechanical loads (combined action).

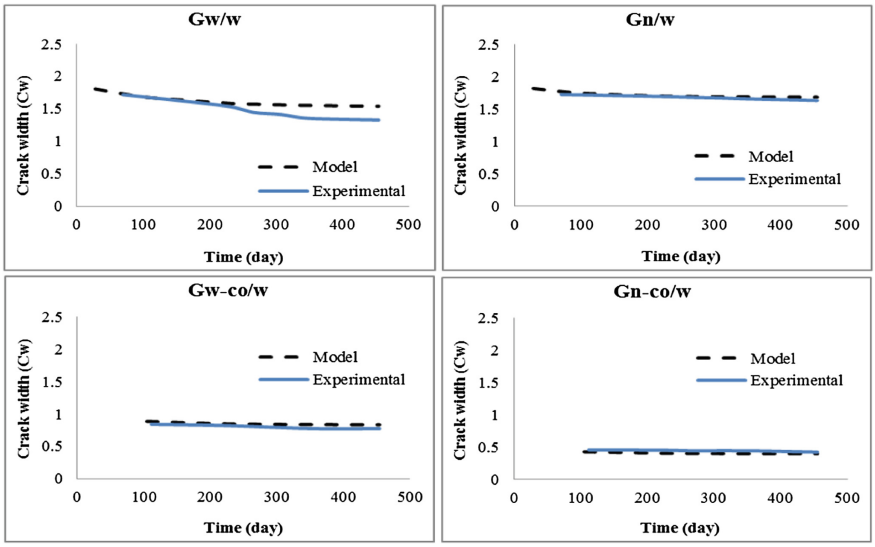

Fig. 15. Experimental and modelled mechanical crack width change under ASR expansion.

6 Conclusions

ASR deterioration under accelerated conditions according to ASTM C1260 was tested on reinforced concrete prisms containing high alkaline (NaOH). Half of them were exposed to cyclic loading causing a macro-crack in the middle, referred to as combined action (mechanical and ASR). The other half were not mechanically cracked but kept under the same accelerated ASR exposure conditions. Four concrete mixes were tested in this way, namely a mix: (i) with Greywacke coarse aggregate denoted (Gw) as reactive aggregate, (ii) one with Granite denoted (Gn) as non-reactive aggregate, and mixes (iii) and (iv) the same aggregates as in (i) and (ii), but with 50% of the cement by weight replaced with ground granular corex slag (GGCS) denoted (co). In the specimens subjected to the combined action, cracks of width in the range 0.6 mm to 1.8 mm were induced by a tensile cyclic load named "combined" and unloaded named "ASR" specimens. Then all specimens were partially submerged in water at 38 °C temperature, and the upper half was exposed to >90% humidity. The following conclusions are drawn from the results obtained during 65 weeks of ASR exposure:

1 Mechanical cracks play a significant role in concrete strain due to the ASR. The macro-cracks in the middle of specimens were reduced due to the freedom this region offers for ASR swelling-induced deformation.
2 The reduction in mechanical crack width was clearly the largest in specimens with greater ASR reactivity, in this case, the Gw specimens. Also, adding 50% of GGCS as a cementitious bender led to a reduction in reactivity, and less reduction in the crack width. This was particularly clear in the Gw-co specimens, compared with the Gw specimens. In the Gn-co specimens the least expansion was found in the Gn-co specimens, and in these specimens, the mechanical crack width reduced insignificantly.
3 The mechanism of concrete expansion and the mechanical crack reduction was modeled in terms of ASR extent and initial mechanical crack width. The models produce results in reasonable agreement with the overall ASR-induced deformation of the samples, besides development in time of the central mechanical crack width.

References

ASTM C1293: Determination of length change of concrete due to alkali-silica reaction, annual book of ASTM standards. American Society for Testing and Materials (ASTM), United States (2008)

Bangert, F., Meschke, G.: A coupled hygro-chemo-mechanical damage model for ASR-affected concrete. Institute for Structural Mechanics, Ruhr University Bochum, Germany (2001)

Charpin, L., Ehrlacher, A.: A computational linear elastic fracture mechanics-based model for alkali-silica reaction. Cem. Concr. Res. **42**(4), 613–625 (2012). http://doi.org/10.1016/j.cemconres.2012.01.004

Davis, D., Alexander, W.: Properties of Aggregate in Concrete (Vol. Part 1). Hippo Quarries Technical Publication, South Africa (1989)

Davis, D., Coull, W.: Alkali-Aggregate Reaction, vol. 2. Hippo Quarries Technical Publication, South Africa (1991)

Ulm, F.-J., Coussy, O., Li Kefei, C.L.: Thermo-chemo-mechanics of ASR expansion concrete structures. J. Eng. Mech. **126**(March), 233–242 (2000)

Giordano, L., Mancini, G., Tondolo, F.: Durability of R/C structures under mechanical and environmental action. Key Eng. Mater. **462–463**, 949–954 (2011). http://doi.org/10.4028/www.scientific.net/KEM.462-463.949

Ichikawa, T.: Alkali-silica reaction, pessimum effects and pozzolanic effect. Cem. Concr. Res. **39** (8), 716–726 (2009). http://doi.org/10.1016/j.cemconres.2009.06.004

Steffens, A., Li, K., Coussy, O.: Aging approach to water effect on alkali–silica reaction degradation of structures. J. Eng. Mech. **129**(1), 50–59 (2003). http://doi.org/10.1061/(ASCE)0733-9399(2003)129:1(50)

Ahmed, T.M.A., Burley, E., Rigden, S.R.: The effect of alkali-silica-reaction on the fatigue behaviour of plain concrete tested in compression, indirect tension and flexure. Mag. Concr. Res. **51**(6), 375–390 (1999). http://doi.org/10.1680/macr.2001.53.5.353

Wang, K., Jansen, D.C., Shah, S.P., Karr, A.F.: Permeability study of cracked concrete. Cem. Concr. Res. **27**(3), 381–393 (1997)